coatings

MDPI

Article

Comparative Study on Microstructures and Wear Properties of Laser-Clad AlCoCrFeNi High-Entropy Alloy Coating and TiC/AlCoCrFeNi Composite Coating

Lianmeng Wang [1], Jianke Luo [1], Jiang Wang [1], Ying Xu [1], Hui Dong [2] and Yongsheng Zhu [2,*]

[1] Shaanxi WeiHe Power Station Co., Ltd., Xi'an 710065, China; wlm19691223@163.com (L.W.); ljk2387@163.com (J.L.); 13629293171@163.com (J.W.); 13891990927@163.com (Y.X.)
[2] School of Materials Science and Engineering, Xi'an Shiyou University, No. 18, Dianzi 2nd Road, Xi'an 710065, China; donghui@xsyu.edu.cn
* Correspondence: zhuys@xsyu.edu.cn; Tel.: +86-029-88382607

Abstract

Steel components in thermal power plants are vulnerable to severe wear and wall thinning induced by the high-velocity impact of pulverized coal, which significantly compromises their service life and structural integrity. To address this issue, a TiC-reinforced AlCoCrFeNi high-entropy alloy (HEA) composite coating was fabricated via laser cladding, aiming to substantially enhance the wear resistance of these critical components. The phase composition, microstructure, microhardness and tribological behaviors of the coatings were systematically investigated by XRD, SEM, EDS and dry sliding wear tests. Results show that both coatings possess dense microstructures and reliable metallurgical bonding with the substrate. The AlCoCrFeNi coating consists of a single BCC solid solution phase, while the TiC/AlCoCrFeNi composite coating contains a BCC phase and a TiC ceramic phase without brittle intermetallic compounds. The average microhardness of the TiC/AlCoCrFeNi composite coating was measured to be 823 $HV_{0.3}$, which is 85.66% greater than that of the AlCoCrFeNi coating (443 $HV_{0.3}$). Under identical wear test conditions, the AlCoCrFeNi coating exhibits a mass loss of 31.4 mg and a volumetric wear rate of 24 $\times$ 10^{-3} mm^3/min, whereas the TiC/AlCoCrFeNi composite coating exhibits a mass loss of 15.6 mg and a wear rate of 13 $\times$ 10^{-3} mm^3/min, corresponding to reductions of approximately 50.32% and 45.83%, respectively. The wear mechanism of the AlCoCrFeNi coating is dominated by severe abrasive wear coupled with adhesive wear, while the addition of TiC converts the wear mechanism into mild abrasive wear and oxidative wear. The incorporation of TiC particles effectively enhances the microhardness and reduces the mass loss, thereby contributing to a marked improvement in the wear properties of the laser-clad AlCoCrFeNi coating. This research provides experimental data and theoretical support for the engineering application of TiC/AlCoCrFeNi composite coatings on wear-resistant components in thermal power units.

Keywords: high entropy alloys; laser cladding; titanium carbide; microhardness; wear

Check for updates

Academic Editor: Lech Pawlowski

Received: 24 June 2026
Revised: 14 July 2026
Accepted: 16 July 2026
Published: 17 July 2026

Copyright: © 2026 by the authors. Licensee MDPI, Basel, Switzerland. This article is an open access article distributed under the terms and conditions of the Creative Commons Attribution (CC BY) license.

1. Introduction

Key components of thermal power generation systems, including boiler pipelines and fan impellers, operate for prolonged periods under extremely harsh service conditions. These components are concurrently exposed to high-speed pulverized coal erosion, abrasive wear and cyclic alternating loads, rendering wear failure the predominant failure

mechanism for thermal power equipment [1–3]. Severe material wear directly causes tube wall thinning, pipeline leakage and even catastrophic pipe rupture, which in turn triggers unplanned unit outages [4–6]. Extensive operational data demonstrate that such wear-induced forced outages not only substantially escalate the operation and maintenance expenditures of thermal power plants, but also critically undermine the safe and continuous operation of generating units [7]. Accordingly, developing high-performance anti-wear protective technologies for critical power equipment has become an urgent technical requirement for the performance improvement and operational optimization of modern thermal power units.

Surface modification is one of the effective strategies for improving the surface performance of metallic components [8,9]. This technique can endow component surfaces with superior wear and corrosion resistance while preserving the bulk mechanical properties of the substrate. It avoids the replacement of large structural components and thus offers distinct economic and technical advantages for industrial applications. Among diverse surface modification technologies, laser cladding exhibits outstanding technical competitiveness owing to its inherent characteristics. It features high energy density and rapid solidification kinetics, which enable the formation of sound metallurgical bonding between the deposited coating and the substrate. Furthermore, this technique allows precise localized strengthening and selective defect repair of key components [10–12]. Benefiting from these advantages, laser cladding has been widely adopted for surface reinforcement of critical complex components in thermal power industries. Nevertheless, conventional nickel-based [13], cobalt-based [14], and iron-based [15] alloy cladding coatings still suffer from significant performance limitations under extreme working conditions involving high-temperature erosion and thermal fatigue. These traditional coatings cannot achieve a balanced combination of hardness, toughness, and oxidation resistance. Coating spalling frequently occurs during long-term service, leading to unsatisfactory performance and a short service life, which greatly restricts their large-scale engineering application.

As an emerging class of multi-principal element alloys, high-entropy alloys (HEAs) possess four core characteristics, namely high mixing entropy, sluggish atomic diffusion, severe lattice distortion and the cocktail effect of multiple alloying elements [16–18]. These unique features allow HEAs to preferentially form simple solid-solution phases and effectively suppress the precipitation of brittle intermetallic compounds, which is a common issue in traditional single-principal alloys. In addition, HEAs exhibit a combination of outstanding properties, such as high hardness, excellent thermal stability, superior corrosion resistance, and a good balance of strength and toughness. Accordingly, HEAs have become promising coating materials for overcoming the performance limitations of conventional laser-clad coatings [19–21].

Among the various HEA systems, AlCoCrFeNi has attracted extensive research attention owing to its compositional simplicity and widely tunable microstructure and mechanical properties [22,23]. Chromium element can form a dense and continuous protective oxide film on the coating surface, which significantly improves the corrosion resistance of the material [24]. Cobalt and nickel elements synergistically guarantee the ductility of the coating and maintain microstructural stability at elevated temperatures [25]. Aluminum facilitates the formation of body-centered cubic (BCC) phase, which further elevates the yield strength of the alloy [26]. Combined with the rapid non-equilibrium solidification feature of laser cladding technology, laser-clad AlCoCrFeNi coatings can achieve synergistic strengthening from grain refinement and solid-solution strengthening. Their comprehensive performance is far superior to that of traditional stainless steels such as 304 and 316L. Given these advantages, AlCoCrFeNi coating is regarded as an ideal candidate material for anti-wear protective coatings used in thermal power plants.

Despite the overall superior performance of AlCoCrFeNi HEAs, single-phase laser-clad AlCoCrFeNi coatings suffer from significant performance shortcomings under the harsh service conditions of thermal power equipment, where severe pulverized coal erosion and reciprocating dry friction prevail. The microstructure of AlCoCrFeNi coatings primarily consists of a body-centered cubic (BCC) phase, an ordered BCC phase, and a minor fraction of face-centered cubic (FCC) phase. Their strengthening mechanisms rely solely on solid-solution strengthening and grain refinement strengthening, which endows the coatings with relatively low microhardness. Under the combined action of particle cutting and repeated plowing from external abrasives, the coating is prone to plastic deformation and surface spalling. Meanwhile, cyclic contact stress will initiate and propagate fatigue cracks inside the coating, which further increases the wear rate. Consequently, monolithic AlCoCrFeNi HEA coatings fail to satisfy the long-life anti-wear and safety protection requirements of key components in thermal power plants [27–29].

The incorporation of hard ceramic particles into metallic matrices to form metal matrix composite coatings is a well-established strategy for improving the hardness and wear resistance of laser-clad coatings [30]. Xie [31] and Li [32] et al. incorporated WC secondary particles into HEA coatings by mechanical alloying, and found that the WC reinforcement effectively elevated the hardness and wear resistance of the as-prepared coatings. Nevertheless, severe decomposition and decarburization easily occur to WC in the high-temperature laser molten pool. A large number of free W and C atoms are consequently released. The diffused W atoms can readily react with Cr and Fe elements. This reaction produces brittle W-rich intermetallic carbides, including W_2C and $(W,Cr)_2C$. A thick brittle reaction layer thus forms around each ceramic particle. These brittle interfacial layers greatly elevate the residual internal stress of the coating. High residual stress further induces microcrack nucleation and surface spalling of the cladding layer. Titanium carbide (TiC) stands out as a popular ceramic reinforcement owing to its ultrahigh hardness, high melting temperature, outstanding abrasion resistance and stable chemical inertness. Critically, TiC possesses favorable wettability with multi-principal-element metallic matrices, which facilitates the formation of robust metallurgical interfaces between the ceramic reinforcement and HEA matrix during laser deposition [33,34].

Nevertheless, most existing literature [35,36] introduces TiC secondary phases into AlCoCrFeNi coatings via in situ synthesis. This route fails to achieve precise regulation over TiC volume fraction. Excess Ti solute atoms may therefore trigger uncontrolled precipitation of brittle phases, which deteriorates the comprehensive performance of the as-fabricated coatings. Based on the above analysis, in this study, TiC particles with a mass fraction of 50% were combined with AlCoCrFeNi powder through mechanical mixing.

To meet the practical engineering requirements for anti-wear applications in thermal power equipment, TiC/AlCoCrFeNi composite coatings were fabricated on Q235 steel substrates via laser cladding in this work. The effects of TiC particle addition on phase composition, microstructure, microhardness, and tribological properties of the coatings were systematically investigated. Furthermore, the evolution mechanism of wear failure in the composite coatings was analyzed. The findings of this work are expected to provide a theoretical basis and technical support for the engineering application of TiC/AlCoCrFeNi composite coatings on anti-wear components in thermal power industries.

2. Materials and Methods

2.1. Materials

Commercial Q235 steel plates (5 mm in thickness and 25.4 mm in diameter; Baosteel Co., Ltd., Shanghai, China) were selected as the laser cladding substrate, as this alloy is extensively applied to fabricate critical wear-prone structural components in thermal power

units. The chemical composition (mass fraction) of the Q235 steel is summarized in Table 1. Prior to cladding fabrication, systematic surface pretreatment was implemented to eliminate surface contaminants. First, the substrate surfaces were mechanically abraded using silicon carbide abrasive papers to remove oxide scales and superficial defects. Afterwards, the polished specimens underwent ultrasonic degreasing in anhydrous ethanol for 15 min. Following natural air drying, all pretreated substrates were stored inside a desiccator until further use. The above pretreatment procedures guaranteed the high-quality metallurgical bonding between the cladding coating and steel substrate.

Table 1. Chemical composition of Q235 steel.

Elements	C	Si	Mn	S	P	Fe
wt.%	≤0.22	≤0.35	≤1.4	≤0.056	≤0.045	bal.

Gas-atomized spherical AlCoCrFeNi high-entropy alloy powder (45–105 μm; Shandong Baobo Material Technology Co., Ltd., Shandong, China) was used as the primary cladding material.The surface morphology of pure AlCoCrFeNi powder is presented in Figure 1a. The composite powder displays a regular spherical morphology with particle diameters ranging from 45 μm to 105 μm, satisfying the particle size criteria for coaxial powder feeding during laser cladding. The chemical composition (mass fraction) of the gas-atomized AlCoCrFeNi powder is summarized in Table 2. The results verify the high purity of the powder fabricated by direct gas atomization, with no obvious precipitation of impurity elements observed. Titanium carbide (TiC) powder was purchased from Shanghai Aladdin Biochemical Technology Co., Ltd., Shanghai, China and used as the ceramic reinforcing phase in this work. As shown in Figure 1b, TiC particles present an irregular granular morphology, containing both microscale and nanoscale grains, which is conducive to the dispersion strengthening effect in the metal matrix.

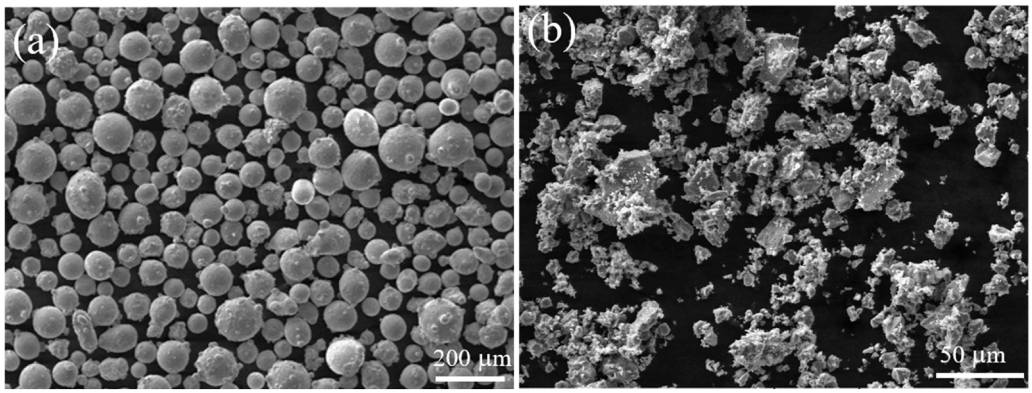


Figure 1. Morphology of raw powder materials: (**a**) AlCoCrFeNi high-entropy alloy powder; (**b**) Mixed TiC/AlCoCrFeNi composite powder.

Table 2. Chemical composition of AlCoCrFeNi high-entropy alloy powder.

Elements	Al	Co	Cr	Fe	Ni
wt.%	10.71	24.51	20.37	21.56	22.85

2.2. Powder Mixing and Pretreatment

AlCoCrFeNi powder and TiC ceramic powder were mixed at a mass ratio of 1:1. The powder mixing process was carried out in a 400 mL agate milling jar via planetary ball milling. The weight ratio of grinding balls to mixed powder was set as 8:1, the rotational

speed of the ball mill was 200 r/min, and the total milling time was 30 min. After ball milling, the two powders were fully blended to obtain uniform composite powder.

To remove adsorbed moisture from the powder surface and ensure stable powder flowability during laser cladding, the mixed composite powder was dried in an electric thermostatic forced-air drying oven (DHG101-5A, Xi'an Yuhui Instrument Co., Ltd., Xi'an, China) at 120 °C for 3 h.. The drying temperature was set at 120 °C, and the drying duration was 3 h. The dried powder was sealed and stored for subsequent laser cladding experiments.

2.3. Laser Cladding Process

All laser cladding experiments were conducted in a sealed atmosphere-controlled chamber to isolate air and avoid high-temperature oxidation of the molten coating. Before the experiment, the chamber was firstly evacuated to a low vacuum state, and then filled with high-purity argon as the shielding gas. The oxygen content inside the chamber was strictly controlled below 50 ppm throughout the cladding process, which effectively prevented the oxidation of molten metal and ceramic phases. The main technological parameters of laser cladding are summarized in Table 3.

Table 3. Laser cladding process parameters.

Parameters	Value
Laser power(W)	800
Laser spot diameter (mm)	3
Speed (mm/s)	3
Scanning strategy	Unidirectional linear scanning
Shielding gas (high-purity Ar) flow rate (L/min)	15
Laser energy density (J/mm^2)	88.89
Overlapping (%)	50
Feed rate (g/min)	6

2.4. Characterization

The phase composition of AlCoCrFeNi coating and TiC/AlCoCrFeNi composite coating was analyzed by an The phase compositions of the AlCoCrFeNi coating and the TiC/AlCoCrFeNi composite coating were characterized using an X-ray diffractometer (XRD-6000, Shimadzu Corporation, Kyoto, Japan).The cross-sectional microstructures of the coatings and the surface morphologies of the worn samples were examined using a field-emission scanning electron microscope (MIRA4, TESCAN, Brno, Czech Republic). The elemental distributions and local chemical compositions of the coatings were analyzed using an attached energy-dispersive X-ray spectrometer (EDS; model, Oxford Instruments, Abingdon, UK). was used to test the elemental distribution and chemical composition of local micro-regions on the coatings.

The cross-sectional microhardness of coatings was measured using an The cross-sectional microhardness of the coatings was measured using a Vickers microhardness tester (KHVS-1000D, Zhejiang Kebiao Technology Co., Ltd., Jiaxing, China). The applied indentation load was 300 g, and the load holding time was 15 s. Along the longitudinal cross-section of the coating, microhardness tests were continuously carried out from the coating surface to the Q235 steel substrate with a test interval of 0.1 mm. Three indentations were tested at each test position to reduce experimental error, and the average value of three test data was taken as the final microhardness result.

The wear properties of the coatings were evaluated by dry sliding wear tests on an The wear properties of the coatings were evaluated by dry sliding wear tests conducted using a multifunctional tribometer (MMX-3G, Jinan Hengxu Testing Machine Technology

Co., Ltd., Jinan, China) in a pin-on-disc contact configuration. with a pin-on-disk contact configuration. The laser-clad samples were processed into pin-shaped specimens as the upper friction pair, and commercial 45# steel disk was used as the lower counter friction pair. The wear test parameters were set as follows: normal load 40 N, disk rotational speed 100 r/min, total test time 30 min. Before and after each wear test, all specimens were ultrasonically cleaned with anhydrous ethanol to remove surface wear debris and contaminants. All dry sliding wear tests were performed under laboratory ambient conditions of 25 °C and 50% relative humidity (RH). The total sliding distance for each test reached 113.0 m, and three parallel specimens were tested for each coating group to guarantee experimental repeatability. A high-precision electronic analytical balance was adopted to measure the mass loss of the samples. The friction coefficient was recorded in real time during the test. Once the tribological test was finished, the volumetric wear rate was calculated by dividing the total wear volume loss by the total sliding duration. The structural schematic of the pin-on-disk tribometer is shown in Figure 2. It should be noted that the coating surface was polished prior to the wear test, and three parallel specimens were prepared for each sample, with the average value calculated to ensure the accuracy of the test results.

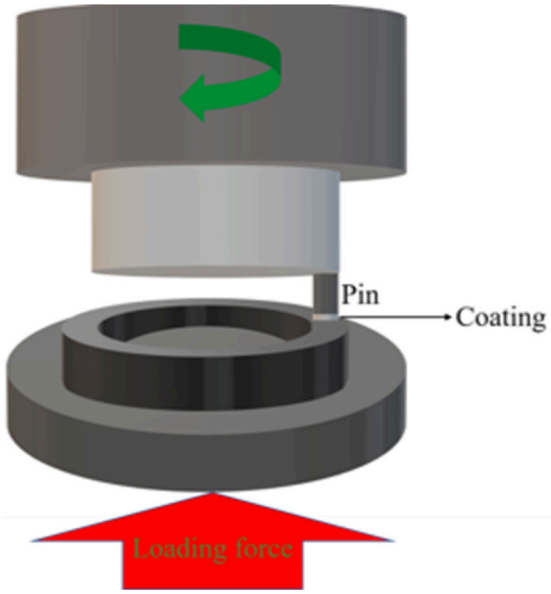


Figure 2. Schematic diagram of the pin-on-disk dry sliding wear tester.

3. Results

3.1. Microstructure

The cross-sectional microstructure of laser-clad AlCoCrFeNi coating is displayed in Figure 3a,b. As observed from the SEM images, the AlCoCrFeNi coating presents a uniform and dense microstructure without typical metallurgical defects such as pores, shrinkage cavities and penetrating cracks. The continuous and tight interface is formed between the cladding coating and Q235 steel substrate, which indicates that high-quality metallurgical bonding is achieved between the coating and substrate after laser cladding. EDS elemental analysis was performed on the cross-section of AlCoCrFeNi coating. The test results (as shown in Figure 3c) reveal that the atomic ratio of the main alloying elements (Al, Co, Cr, Fe, Ni) in the coating is approximately 1:1, which is basically consistent with the element ratio of the original gas-atomized HEA powder. Meanwhile, considerable Fe enrichment is identified within the deposited coating. This observation can be attributed to the intense thermal effect induced by the high-energy laser beam. Upon high-intensity laser irradiation, a thin superficial layer of the Q235 steel substrate undergoes partial melting. Interdiffusion

of constituent elements takes place between the molten substrate and liquid cladding powder during the subsequent solidification stage, which ultimately results in prominent Fe accumulation throughout the coating matrix.

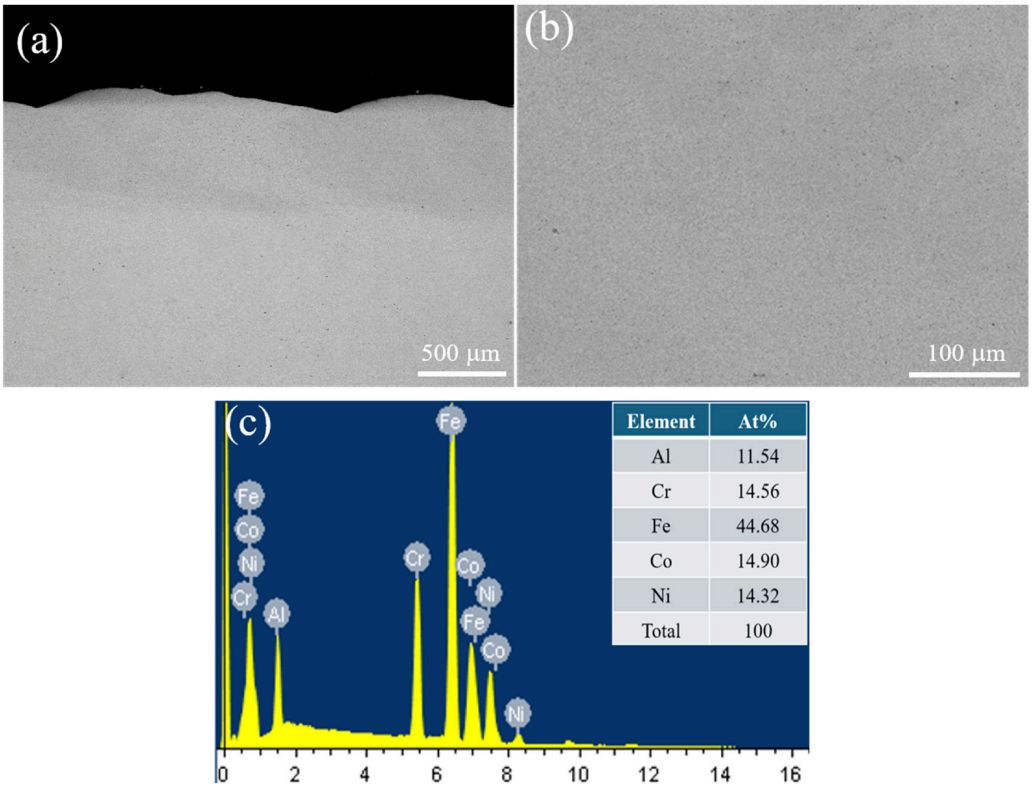


Figure 3. Cross-sectional microstructures of laser-clad AlCoCrFeNi coating: (**a**) low magnification microstructure; (**b**) high magnification microstructure; (**c**) EDS elemental analysis results of AlCoCrFeNi coating.

After adding TiC reinforcing particles, the cross-sectional microstructure of TiC/AlCoCrFeNi composite coating is shown in Figure 4. Similarly, the composite coating still maintains a dense microstructure, and the coating-substrate interface remains intact without defects. Two characteristic microzones with disparate grayscale contrast are clearly distinguishable in the SEM micrographs. The gray matrix domain corresponds to the AlCoCrFeNi matrix phase, whereas the discrete dark precipitates represent the secondary reinforcing phase. Combined with EDS point analysis and elemental mapping, the dark phase exhibits prominent Ti and C segregation, unambiguously verifying its identity as TiC ceramic particles. These TiC particulates achieve homogeneous distribution throughout the HEA matrix, which provides a prerequisite for the realization of effective dispersion strengthening.

The XRD patterns of AlCoCrFeNi coating and TiC/AlCoCrFeNi composite coating are presented in Figure 5. For the AlCoCrFeNi coating, only the characteristic diffraction peaks corresponding to body-centered cubic (BCC) solid solution phase are detected in the XRD pattern, proving that the coating is composed of a single BCC solid solution phase. For the TiC/AlCoCrFeNi composite coating, besides the diffraction peaks of BCC solid solution phase, obvious characteristic peaks of TiC ceramic phase are also observed. No diffraction peaks of brittle intermetallic compounds or other new impurity phases appear in the composite coating. The above XRD results demonstrate that the introduction of TiC particles does not change the inherent phase structure of AlCoCrFeNi HEA matrix, and the interface between BCC matrix and TiC phase keeps stable during laser cladding.

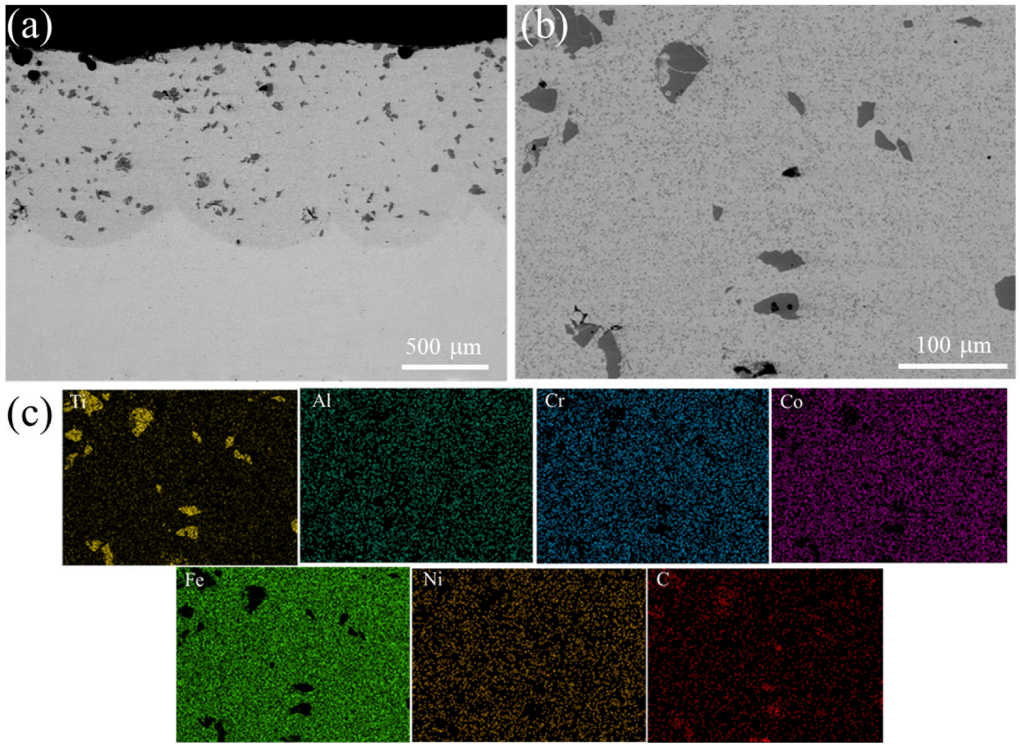


Figure 4. Cross-sectional microstructures of laser-clad TiC/AlCoCrFeNi composite coating: (**a**) low magnification microstruc-ture; (**b**) high magnification microstructure; (**c**) EDS elemental distribution mapping.

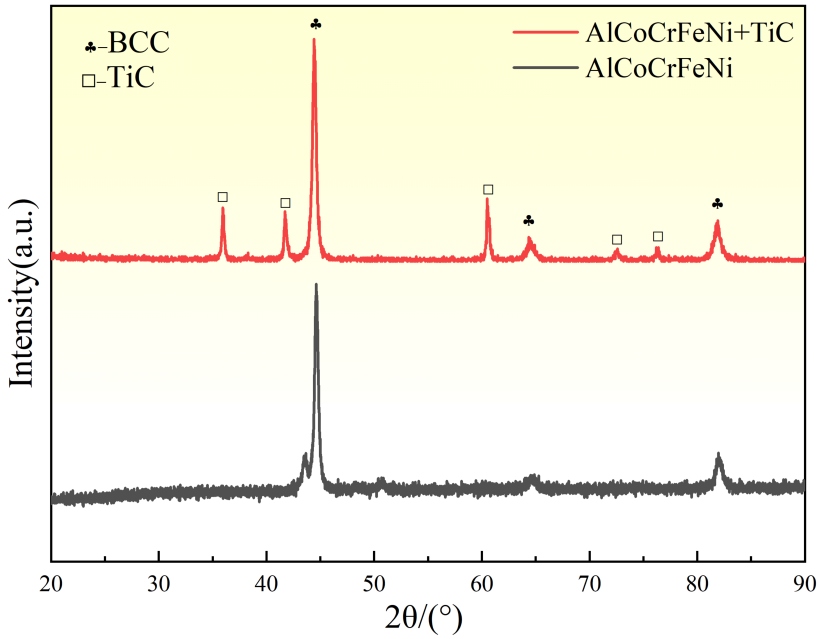


Figure 5. XRD patterns of the AlCoCrFeNi coating and the TiC/AlCoCrFeNi composite coating.

3.2. Microhardness

Figure 6a shows the cross-sectional microhardness distribution curves of AlCoCrFeNi coating and TiC/AlCoCrFeNi composite coating. For both two types of laser-clad coatings, the microhardness presents an obvious stepwise variation trend from the coating surface to the Q235 steel substrate. Within the cladding layer area, the microhardness value remains relatively high and stable. At the coating-substrate interface region, the microhardness

drops sharply, and finally gradually approaches the microhardness value of the base steel substrate.

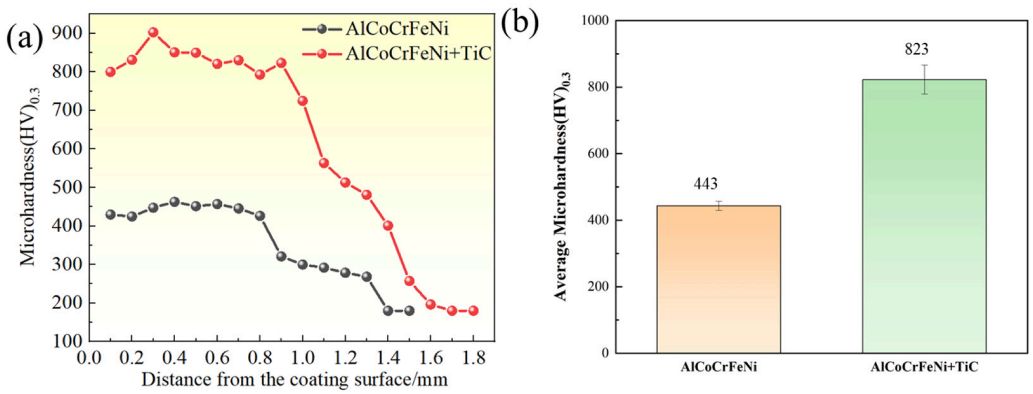


Figure 6. Microhardness of coatings: (**a**) microhardness curves of the coatings; (**b**) average microhardness of the coatings.

Figure 6b compares the average microhardness of the two coatings. It can be found that the uniformly dispersed TiC ceramic particles produce an obvious dispersion strengthening effect, which greatly improves the overall microhardness of the composite coating. The average microhardness of the AlCoCrFeNi coating is measured to be 443 $HV_{0.3}$. In stark comparison, the TiC-reinforced AlCoCrFeNi composite coating delivers an average microhardness of 823 $HV_{0.3}$, representing an approximately 85.66% enhancement relative to the monolithic HEA counterpart. This prominent performance improvement originates from the uniform distribution of intrinsically hard titanium carbide (TiC) particulates throughout the metallic matrix. These ceramic reinforcements can directly bear externally applied loads and efficiently suppress dislocation motion within the matrix, which substantially elevates the microhardness of the cladding layer. It is worth noting that the increase in microhardness lays the foundation for the excellent wear properties of the AlCoCrFeNi coating. According to Wu et al. research [37], higher microhardness can effectively inhibit the plastic deformation of the friction contact surface, reduce abrasive etching and the transfer of adhered materials, thereby endowing the composite coating with excellent wear resistance under friction loads.

3.3. Wear Properties

Figure 7 presents the friction coefficient evolution curves of the two coatings acquired under dry sliding wear conditions. The AlCoCrFeNi coating exhibits an average friction coefficient of roughly 0.55, whereas the TiC/AlCoCrFeNi composite coating delivers a lower average value of approximately 0.45. Incorporation of TiC ceramic reinforcements reduces the mean friction coefficient by nearly 18.2%, which mitigates the interfacial frictional resistance throughout the wear process. The TiC-reinforced composite coating shows lower average friction coefficient yet stronger curve fluctuations than AlCoCrFeNi coating. Hard TiC particles periodically detach from the matrix under cyclic shear stress, forming third-body abrasives that cause sharp friction peaks, while their clearance leads to valley values. Alternating contact between soft HEA matrix and protruding TiC grains also disturbs friction stability. In addition, rigid TiC continuously scrapes and breaks the surface tribo-film, and its repeated formation and destruction further amplify cyclic coefficient oscillations during sliding.

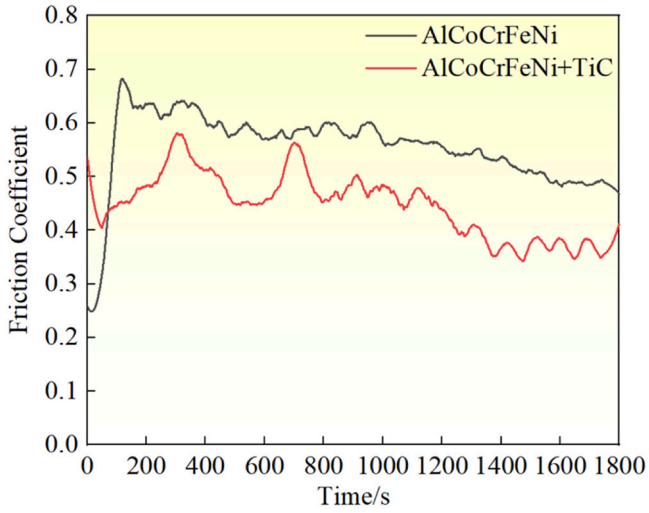


Figure 7. Friction coefficient variation regulation of coatings.

Figure 8 compares the mass loss and volumetric wear rate of the two coatings subjected to 30 min dry sliding wear tests. Experimental measurements reveal that the AlCoCrFeNi coating exhibits a mass loss of 31.4 mg and a volumetric wear rate of 15.6 mm^3/min. By contrast, the TiC/AlCoCrFeNi composite coating merely presents a mass loss of 24 mg and an extremely low volumetric wear rate of 13 × 10^{-3} mm^3/min. Quantitative calculation demonstrates that the mass loss and volumetric wear rate of the composite coating drop by approximately 50.32% and 45.83%, respectively, relative to the HEA counterpart. The reduction in mass loss and wear rate of the TiC/AlCoCrFeNi composite coating is correlated with the dispersion strengthening induced by uniformly distributed TiC particles. The hard TiC ceramic phases distributed within the AlCoCrFeNi coating serve as load-bearing frameworks during dry sliding contact, which can effectively hinder coating plastic flow, suppress abrasive plowing and interfacial adhesive transfer, and weaken material spalling under cyclic frictional shear stress. Collectively, these synergistic strengthening effects greatly reduce the material loss of the coating under reciprocating friction, which firmly verifies that the incorporation of TiC ceramic reinforcements can improve the anti-wear properties of laser-clad AlCoCrFeNi coatings.

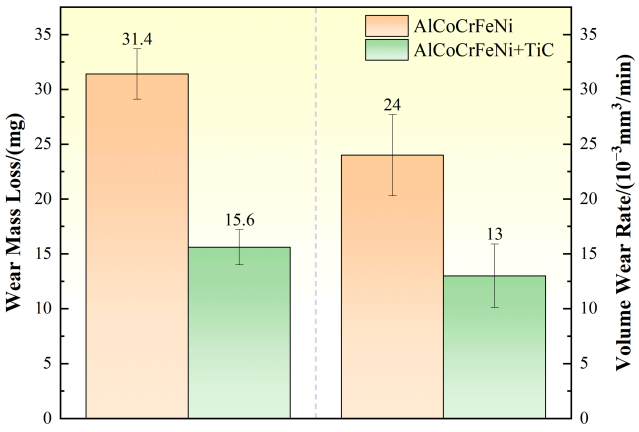


Figure 8. Mass loss and volumetric wear rate of the two coatings.

3.4. Worn Surface Morphology and Wear Mechanism

Figure 9 displays the worn surface morphology of the AlCoCrFeNi coating after dry sliding wear tests. The SEM observations reveal that numerous wide and deep continuous grooves are distributed along the sliding direction of the friction interface(as shown in

Figure 9a). These characteristic grooves are primarily induced by the cutting and plowing behavior of micro-protrusions on the friction pair and detached wear debris, demonstrating that the AlCoCrFeNi coating undergoes severe abrasive wear. Additionally, abundant spalling pits originating from adhesive delamination are clearly visible on the worn surface(as shown in Figure 9b). During continuous sliding, local cold welding readily occurs at the contact interface between the coating and friction pair. Subsequent relative sliding facilitates the peeling and transfer of surface materials, thereby inducing typical adhesive wear features.

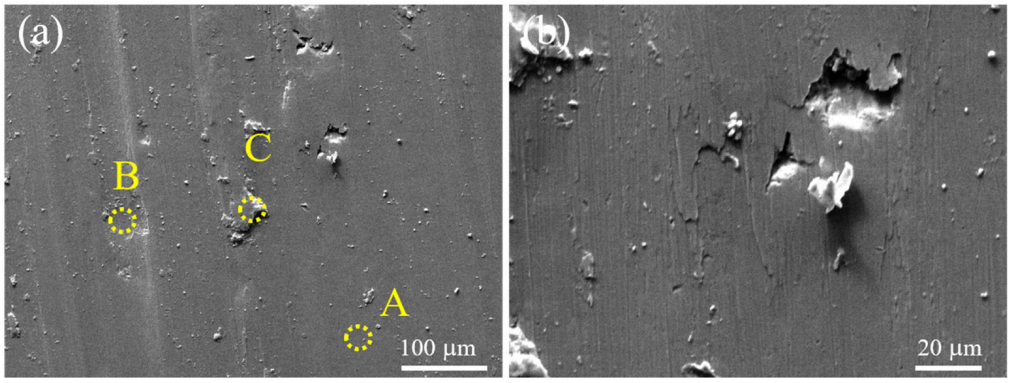


Figure 9. The surface morphology of the AlCoCrFeNi coating after friction and wear tests: (**a**) low magnification morphology; (**b**) high magnification morphology of delamination.

Overall, the wear behavior of the AlCoCrFeNi coating is governed by the synergistic effect of abrasive wear and adhesive wear. The relatively low microhardness of the AlCoCrFeNi coating endows the material with poor resistance to plastic deformation and interfacial adhesion, which ultimately leads to severe surface material loss.

Table 4 summarizes the EDS point analysis results of typical regions on the worn surface of the AlCoCrFeNi coating. Trace oxygen elements are detected within localized wear pits, confirming the occurrence of mild interfacial oxidation during the dry sliding process.

Table 4. EDS elemental composition results of typical regions on the worn surface of AlCoCrFeNi coating (wt.%).

Region/wt.%	Al	Co	Cr	Fe	Ni	O
A	5.92	16.78	14.72	45.78	16.80	-
B	4.82	16.24	14.27	50.14	14.53	-
C	4.24	10.25	9.15	63.49	9.38	3.49

Figure 10 presents the worn surface morphology of the TiC/AlCoCrFeNi composite coating. The incorporation of TiC ceramic reinforcements substantially improves the surface flatness of the worn coating. Although shallow grooves and tiny wear debris are still observable on the wear track, both the depth and width of the grooves are remarkably reduced, indicating that the abrasive wear behavior is effectively restrained. The uniformly dispersed high-hardness TiC particles can sustain the majority of applied loads, inhibit the penetration of abrasive particles into the HEA matrix, and suppress the plowing effect during sliding. Furthermore, no evident adhesive spalling pits are detected on the worn surface of the composite coating, confirming its greatly enhanced resistance to adhesive wear. The improved microhardness of the composite coating suppresses the occurrence of interfacial cold welding and surface material transfer during friction.

Combined with the EDS results listed in Table 5, abundant oxygen is enriched on the worn surface, verifying the formation of a dense protective oxide layer throughout the dry sliding process. Consequently, the wear behavior of the TiC/AlCoCrFeNi composite coating is dominated by mild abrasive wear and oxidative wear.

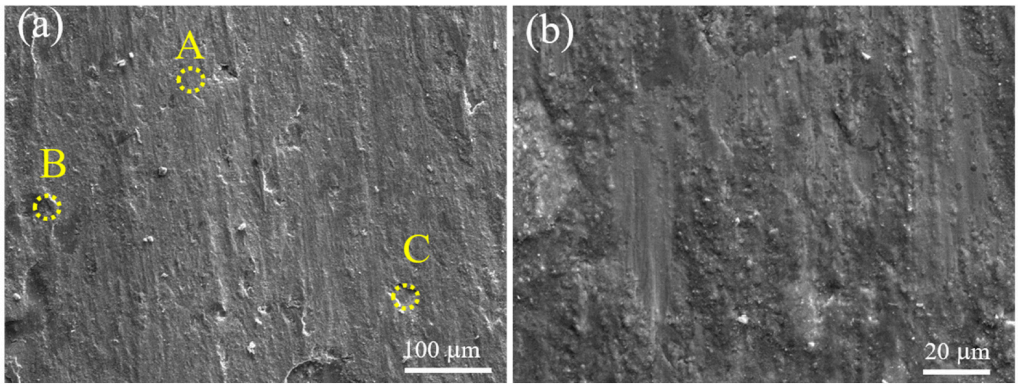


Figure 10. The surface morphology of the TiC/AlCoCrFeNi/TiC coating after friction and wear tests: (**a**) low magnification morphology; (**b**) high magnification morphology.

Table 5. EDS elemental composition results of typical regions on the worn surface of TiC/AlCoCrFeNi composite coating (wt.%).

Region/wt.%	Al	Co	Cr	Fe	Ni	Ti	C	O
A	1.74	5.79	5.61	61.73	4.93	5.28	3.70	11.22
B	0.58	3.35	2.70	66.99	2.90	6.78	6.02	10.68
C	0.11	0.55	-	90.40	0.02	0.48	3.58	4.86

4. Conclusions

In this work, laser cladding was employed to fabricate AlCoCrFeNi coating and TiC/AlCoCrFeNi composite coatings on Q235 steel substrates. The microstructures and wear resistance of the as-fabricated coatings were systematically investigated. The main conclusions are drawn as follows:

1. Both coatings exhibit fully dense microstructures and form sound, defect-free metallurgical bonding with the Q235 steel substrate. XRD analysis verifies that the single-phase AlCoCrFeNi coating contains a BCC solid-solution matrix. Incorporation of TiC ceramic particles introduces discrete TiC reinforcing phases without triggering precipitation of brittle intermetallic compounds or altering the inherent BCC phase constitution of the HEA matrix. The chemically stable TiC/BCC interface eliminates phase incompatibility risks during laser rapid solidification, providing a fundamental structural basis for the mechanical and wear property of the TiC/AlCoCrFeNi composite coatings.
2. Homogeneously dispersed TiC particles deliver prominent dispersion strengthening, which substantially elevates the microhardness and anti-wear capacity of the cladding coating. The TiC/AlCoCrFeNi composite coating achieves an average microhardness of 823 $HV_{0.3}$, representing an 85.66% increment compared with AlCoCrFeNi coating. Meanwhile, its average friction coefficient declines by ~18.2%, accompanied by remarkable reductions in wear mass loss and volumetric wear rate.
3. The low-microhardness single-phase AlCoCrFeNi coating is governed by coupled abrasive and adhesive wear, resulting in severe material loss under heavy-load dry sliding conditions. Embedded TiC particles drastically improve coating microhardness

and resist abrasive cutting and adhesive spalling, switching the dominant wear mechanism to mild abrasive wear coupled with protective oxidative wear. The superior long-term wear stability renders the TiC/AlCoCrFeNi composite coating an ideal candidate surface protection material for coal-fired thermal power components suffering from high-speed pulverized coal erosion.

Author Contributions: Conceptualization, H.D. and Y.Z.; methodology, Y.X.; validation, Y.X., J.W. and J.L.; formal analysis, J.L.; investigation, L.W.; resources, L.W.; data curation, J.W.; writing—original draft preparation, L.W.; writing—review and editing, H.D.; supervision, Y.Z.; project administration, L.W., H.D. and Y.Z. All authors have read and agreed to the published version of the manuscript.

Funding: This research received no external funding.

Institutional Review Board Statement: Not applicable.

Informed Consent Statement: Not applicable.

Data Availability Statement: The raw data supporting the conclusions of this article will be made available by the authors on request.

Conflicts of Interest: Authors Lianmeng Wang, Jianke Luo, Jiang Wang, and Ying Xu were employed by the company Shaanxi WeiHe Power Station Co., Ltd. The remaining authors declare that the research was conducted in the absence of any commercial or financial relationships that could be construed as potential conflicts of interest.

References

1. Nagarajan, R.; Ambedkar, B.; Gowrisankar, S.; Somasundaram, S. Development of predictive model for fly-ash erosion phenomena in coal-burning boilers. *Wear* **2009**, *267*, 122–128. [CrossRef]
2. Abe, F.; Kutsumi, H.; Haruyama, H.; Okubo, H. Improvement of oxidation resistance of 9 mass% chromium steel for advanced-ultra supercritical power plant boilers by pre-oxidation treatment. *Corros. Sci.* **2017**, *114*, 1–9. [CrossRef]
3. Mbabazi, J.G.; Sheer, T.J.; Shandu, R. A model to predict erosion on mild steel surfaces impacted by boiler fly ash particles. *Wear* **2004**, *257*, 612–624. [CrossRef]
4. Vicenzi, J.; Villanova, D.L.; Lima, M.D.; Takimi, A.S.; Marques, C.M.; Bergmann, C.P. HVOF-coatings against high temperature erosion (∼300 °C) by coal fly ash in thermoelectric power plant. *Mater. Des.* **2006**, *27*, 236–242. [CrossRef]
5. Hussainova, I.; Kübarsepp, J.; Shcheglov, I. Investigation of impact of solid particles against hard metal and cermets targets. *Tribol. Int.* **1999**, *32*, 337–344. [CrossRef]
6. Li, M.J.; Tang, S.Z.; Wang, F.L.; Zhao, Q.X.; Tao, W.Q. Gas-side fouling, erosion and corrosion of heat exchangers for middle/low temperature waste heat utilization: A review on simulation and experiment. *Appl. Therm. Eng.* **2017**, *126*, 737–761. [CrossRef]
7. Niu, Y.Q.; Tan, H.Z.; Hui, S.E. Ash-related issues during biomass combustion:Alkali-induced slagging, silicate melt-induced slagging (ash fusion), agglomeration, corrosion, ash utilization, and related countermeasures. *Prog. Energy Combust. Sci.* **2016**, *52*, 1–61. [CrossRef]
8. Amanov, A. Surface engineering-controlled tribological behavior and adhesion strength of Ni-Cr coating sprayed onto carburized AISI 4340 steel substrate. *Surf. Coat. Technol.* **2019**, *370*, 144–156. [CrossRef]
9. Sun, H.R.; Song, B.H.; Sun, X.M.; Cui, X.Q.; Liu, Z.X.; Cong, M.; Sun, M.Y.; Zhu, Z.M.; Tian, Y.C.; Liu, S.Y.; et al. Recent Representative Progress of Surface Coating Technology. *Chem. Rec.* **2025**, *25*, e202500054. [CrossRef] [PubMed]
10. Wang, L.X.; Zhang, C.Y.; Wang, C.C.; Liu, G.; Yan, S.X.; Dong, S.Y. Enhanced tribological performance of laser-cladded In718 coatings: Cladding parameters optimization via thermo-mechanical simulation. *Chin. J. Mech. Eng.* **2026**, 100328. [CrossRef]
11. Zhi, X.L.; Li, C.Y.; Yang, L.P.; Wang, X.H.; Wang, B.; Yu, X.; Du, Q.D.; Li, X.C.; Kou, S.Z. Research progress on crack formation mechanism and suppression strategies of laser cladding coatings. *J. Alloys Compd.* **2026**, *1071*, 188802. [CrossRef]
12. Ren, P.L.; Han, R.B.; Zhang, Y.X.; Jia, Y.F.; Zhou, S.J.; Liang, J.; Wu, H.X.; Hua, K.; Wang, H.F.; Shi, X.J. Self-lubricating behavior of a laser-clad boride-reinforced coating on AlCoCrFeNi2.1 eutectic high-entropy alloy. *Mater. Charact.* **2026**, *238*, 116662. [CrossRef]
13. Xu, L.; Liang, Y.W.; Huang, T.H.; Yang, Z.J.; Sun, Y.L.; Li, M.Z.; Su, C.H.; Xiong, Y.J.; Zhai, R.X.; Song, P.; et al. Wear and corrosion resistance of WC-reinforced nickel-based alloy coating for aircraft landing gears. *J. Mater. Res. Technol.* **2026**, *41*, 7532–7546. [CrossRef]

14. Miao, Q.; Zhang, P.; Cao, S.L.; Ma, W.; Chen, F.R.; Du, Z.X.; Liu, F.; Lu, S.S. Study on the microstructure and wide-temperature-range tribological properties of carbide ceramic modified cobalt-based lubricating composite coatings fabricated by laser cladding. *Wear* **2026**, *599*, 206776. [CrossRef]
15. Li, L.X.; Xue, X.J.; Qu, H.T.; Liu, F.; Liu, L.Q.; Chen, X.Y.; Xu, R.Z. Laser-cladded hBN/Ni-based composite coatings for enhanced wear and corrosion resistance of HT250 cast iron. *Int. J. Electrochem. Sci.* **2026**, *21*, 101302. [CrossRef]
16. Lu, Y.P.; Dong, Y.; Guo, S.; Jiang, L.; Kang, H.J.; Wang, T.M.; Wen, B.; Wang, Z.J.; Jie, J.C.; Cao, Z.Q.; et al. A Promising New Class of High-Temperature Alloys: Eutectic High-Entropy Alloys. *Sci. Rep.* **2014**, *4*, 6200. [CrossRef] [PubMed]
17. Ye, Y.F.; Wang, Q.; Lu, J.; Liu, C.T.; Yang, Y. High-entropy alloy: Challenges and prospects. *Mater. Today* **2016**, *19*, 349–362. [CrossRef]
18. Lu, Y.P.; Dong, Y.; Jiang, H.; Wang, Z.J.; Cao, Z.Q.; Guo, S.; Wang, T.M.; Li, T.J.; Liaw, P.K. Promising properties and future trend of eutectic high entropy alloys. *Scr. Mater.* **2020**, *187*, 202–209. [CrossRef]
19. Wang, Z.; Shi, Y.F.; Liu, Y.L.; Feng, L.; Yu, J.; Shen, Y.W.; An, G.L.; Hua, D.P.; Gao, J.P.; Zhang, B.Y.; et al. Tribo-corrosion performances of high-entropy alloy coatings for biomedical applications: A review. *J. Alloys Compd.* **2026**, *1073*, 189048. [CrossRef]
20. Feng, J.Y.; You, G.Q.; Zhou, P.C.; Wu, C.Y.; Jiang, B. Microstructure evolution and mechanical properties of laser-cladding TiFeNiCuV high-entropy alloy coatings. *Trans. Nonferrous Met. Soc. China* **2025**, *35*, 4197–4216. [CrossRef]
21. Wang, J.W.; Jia, D.Z.; Gao, Q.; Fu, Y.Q.; Wu, X.Q. High-entropy alloy coatings: A systematic review on composition design, microstructural mechanisms, and multifunctional application. *Mater. Des.* **2025**, *258*, 114715. [CrossRef]
22. Zhou, Y.W.; Bi, J.; Jia, X.D.; Liu, D.H.; Yang, Z.Y.; Li, Y.H.; Dong, G.J. Laser-clad Y/Hf-doped AlCoCrFeNi high-entropy alloy coatings: Enhanced wear and molten aluminum corrosion resistance. *Tribol. Int.* **2026**, *215*, 111506. [CrossRef]
23. Sun, Y.Y.; Miao, Q.; Liang, W.P.; Gupta, M.; Jia, F.L.; Xu, J.Y.; Yu, H.Y.; Zang, K. High temperature oxidation-resistant AlCoCrFeNi high entropy alloy coating on TiAl alloy: Role of pre-diffusion on oxidation resistance. *Appl. Surf. Sci.* **2025**, *689*, 162501. [CrossRef]
24. Yue, K.; Wang, L.; Xu, Z.; Cheng, C.L.; Wang, Y.Q.; Fan, Y.; Xu, J.; Wang, Z.J.; Chen, Z. Effect of Ti addition on the microstructure and corrosion behavior of laser cladding AlCoCrFeNi high-entropy alloy coatings. *Vacuum* **2024**, *230*, 113633. [CrossRef]
25. Huang, A.H.; Li, L.; Liu, X.Z.; Zhang, H.; Zhang, X.H.; Lu, J.; Chen, Y.; Zhao, X.F. Phase transformation-induced TGO rumpling failure of an AlCoCrFeNi high-entropy alloy after isothermal oxidation at 1200 °C. *Scr. Mater.* **2024**, *239*, 115817. [CrossRef]
26. Chong, Z.Z.; Sun, Y.N.; Cheng, W.J.; Huang, L.F.; Han, C.Y.; Ma, X.F.; Meng, A. Laser remelting induces grain refinement and properties enhancement in high-speed laser cladding AlCoCrFeNi high-entropy alloy coatings. *Intermetallics* **2022**, *150*, 107686. [CrossRef]
27. Wang, R.T.; Liu, H.; Chen, P.J.; Liu, X.H.; Hao, J.B.; Yang, H.F. Enhancing wear resistance of laser-clad AlCoCrFeNi high-entropy alloy via ultrasonic surface rolling extrusion. *Surf. Coat. Technol.* **2024**, *485*, 130908. [CrossRef]
28. Meghwal, A.; Singh, S.; Anupam, A.; King, H.J.; Schulz, C.; Hall, C.; Munroe, P.; Berndt, C.C.; Ang, A.S.M. Nano- and micro-mechanical properties and corrosion performance of a HVOF sprayed AlCoCrFeNi high-entropy alloy coating. *J. Alloys Compd.* **2022**, *912*, 165000. [CrossRef]
29. Shi, P.Y.; Yu, Y.; Xiong, N.; Liu, M.Z.; Qiao, Z.H.; Yi, G.W.; Yao, Q.Q.; Zhao, G.P.; Xie, E.Q.; Wang, Q.H. Microstructure and tribological behavior of a novel atmospheric plasma sprayed AlCoCrFeNi high entropy alloy matrix self-lubricating composite coatings. *Tribol. Int.* **2020**, *151*, 106470. [CrossRef]
30. Wei, Z.; Wu, Y.P.; Hong, S.; Cheng, J.B.; Qiao, L.; Cheng, J.; Zhu, S.S. Effect of WC-10Co on cavitation erosion behaviors of AlCoCrFeNi coatings prepared by HVOF spraying. *Ceram. Int.* **2021**, *47*, 15121–15128. [CrossRef]
31. Xie, Y.J.; Jiang, W.Y.; Liang, C.P.; Wen, X.; Huang, B.S. WC-TiC particle reinforced laser cladded AlCoCrFeNi2.1 eutectic high-entropy alloy coatings: Microstructural refinement, in-situ phase formation and tuning of mechanical and corrosion properties. *J. Alloys Compd.* **2025**, *1047*, 185109. [CrossRef]
32. Li, Z.S.; Xie, D.Q.; Liu, Y.; Lv, F.; Zhou, K.; Jiao, C.; Gao, X.S.; Wang, D.S.; Liu, Y.J.; Zu, H.C.; et al. Effect of WC on the microstructure and mechanical properties of laser-clad AlCoCrFeNi2.1 eutectic high-entropy alloy composite coatings. *J. Alloys Compd.* **2024**, *976*, 173219. [CrossRef]
33. Li, Y.; Shi, Y.J.; Li, Q.; Zhao, X.J. The influence of laser energy density on microstructure and wear resistance of TiC-AlCoCrFeNi high entropy alloy composites coatings. *Surf. Coat. Technol.* **2026**, *529*, 133487. [CrossRef]
34. Huang, J.; Luo, F.Y.; Zhao, Y.; Shi, W.Q. Preparation of AlCoCrFeNi/W-TiC HEA composite coating by laser cladding. *Mater. Today Commun.* **2024**, *39*, 108677. [CrossRef]
35. Li, Y.; Wang, K.; Fu, H.; Guo, X.; Lin, J. Microstructure and wear resistance of in-situ TiC reinforced AlCoCrFeNi-based coatings by laser cladding. *Appl. Surf. Sci.* **2022**, *585*, 152703. [CrossRef]

36. Wu, C.L.; Xu, T.Z.; Wang, Z.Y.; Zhang, C.H.; Zhang, S.; Ni, C.L.; Zhang, D.X. Laser surface alloying of FeCoCrAlNiTi high entropy alloy composite coatings reinforced with TiC on 304 stainless steel to enhance wear behavior. *Ceram. Int.* **2022**, *48*, 20690–20698. [CrossRef]
37. Cao, Q.; Fan, L.; Chen, H.; Hou, Y.; Dong, L.; Ni, Z. Wear behavior of laser cladded WC reinforced Ni-based coatings under low temperature. *Tribol. Int.* **2022**, *176*, 107939. [CrossRef]

Disclaimer/Publisher's Note: The statements, opinions and data contained in all publications are solely those of the individual author(s) and contributor(s) and not of MDPI and/or the editor(s). MDPI and/or the editor(s) disclaim responsibility for any injury to people or property resulting from any ideas, methods, instructions or products referred to in the content.